

UC Berkeley

UC Berkeley Previously Published Works

Title

Effect of Spin-Orbit Coupling on Phonon-Mediated Magnetic Relaxation in a Series of Zero-Valent Vanadium, Niobium, and Tantalum Isocyanide Complexes

Permalink

<https://escholarship.org/uc/item/0wk5q4td>

Journal

Inorganic Chemistry, 60(23)

ISSN

0020-1669

Authors

Chakarawet, Khetpakorn
Atanasov, Mihail
Ellis, John E
[et al.](#)

Publication Date

2021-12-06

DOI

10.1021/acs.inorgchem.1c03173

Peer reviewed

Effect of Spin-Orbit Coupling on Phonon-Mediated Magnetic Relaxation in a Series of Zero-Valent Vanadium, Niobium, and Tantalum Isocyanide Complexes

Khetpakorn Chakarawet, Mihail Atanasov, John E. Ellis, Wayne W. Lukens Jr., Victor G. Young Jr., Ruchira Chatterjee, Frank Neese*, and Jeffrey R. Long*

ABSTRACT: Spin-vibronic coupling leads to spin relaxation in paramagnetic molecules, and understanding factors that contribute to this phenomenon is essential for designing next generation spintronics technology, including single-molecule magnets and spin-based qubits, wherein long-lifetime magnetic ground states are desired. We report spectroscopic and magnetic characterization of the isoelectronic and isostructural series of homoleptic zerovalent transition metals triad $M(\text{CNDipp})_6$ ($M = \text{V}, \text{Nb}, \text{Ta}$; $\text{CNDipp} = 2,6\text{-diisopropylphenyl isocyanide}$), and show experimentally the significant increase in spin relaxation rate upon going from V to Nb to Ta. Correlated electronic calculation and first principle spin-phonon computation support the role of spin-orbit coupling in modulating spin-phonon relaxation. Our results provide experimental evidence that increasing magnetic anisotropy through spin-orbit coupling interactions leads to increased spin-vibronic relaxation which is detrimental to long spin lifetime in paramagnetic molecules.

Introduction

Spin relaxation in paramagnetic molecules is a fundamental phenomenon that plays an important role in diverse fields such as magnetic resonance imaging,¹ single-molecule magnetism,² and quantum information technology.³ There are many possible mechanisms through which spin relaxation can occur. For systems with total electron spin $S > 1/2$, relaxation may occur from a thermal excited state via a mechanism known as the Orbach process.⁴ The corresponding relaxation rate exhibits an Arrhenius temperature-dependence with an activation energy determined by the thermal barrier to spin inversion, U , which is governed by zero-field splitting (for transition metal complexes)⁴ or ligand field splitting (for lanthanide complexes).⁵ At very low temperatures where thermal energy $k_B T \ll U$, the molecular spin can be trapped in its ground state, resulting in magnetic polarization akin to bulk magnets, a property of so-called single-molecule magnets.⁶

Slow magnetic relaxation in single-molecule magnets falls within two classes, namely *spin-phonon* relaxation, such as Orbach, Raman, direct, and local mode processes, and *spin-spin* relaxation, such as hyperfine-mediated and dipole-mediated quantum tunneling of the magnetization.⁷ All of these relaxation mechanisms ultimately result in loss of spin polarization that is necessary for the proposed applications for single-molecule magnets,⁸ and thus research has focused extensively on increasing U and/or minimizing the other relaxation pathways in these molecules. Spin-spin relaxation, especially quantum tunneling of the magnetization, has been extensively studied in molecular systems,⁹ and application of a magnetic field¹⁰ or dilution of magnetic molecules in diamagnetic matrix¹¹ are key strategies for suppressing this process. On the other hand, spin-phonon relaxation, which is mediated

by coupling of electron spin to phonon modes of the solid, is more difficult to control, apart from the well-understood Orbach process.

Recent studies have suggested that intramolecular vibrations are responsible for mediating spin-phonon relaxation in most mononuclear magnets in the temperature regime of interest (~tens of K), hereafter referred to as spin-vibronic relaxation, also known as local mode process.¹²⁻¹⁷ It should be noted that such spin-phonon coupling has recently been applied to describe Raman relaxation process as well.^{18,19} Despite such knowledge, spin-vibronic relaxation nonetheless remains difficult to control experimentally. The elimination of low-frequency molecular vibrational modes has been proposed as one strategy to minimize spin-vibronic relaxation,¹³ but systematic experimental investigations validating this approach are lacking, in large part due to the challenges inherent in achieving systematic control over molecular vibrations while maintaining the electronic structure of the metal center. For example, it has been shown that replacing the tetra(isopropyl)cyclopentadienyl ligand in $[\text{Dy}(\text{Cp}^{\text{iPr4}})_2]^+$ with tetra(isopropyl)methylcyclopentadienyl results in a substantial increase in the 100-s magnetic blocking temperature from 17 K in $[\text{Dy}(\text{Cp}^{\text{iPr4}})_2]^+$ to 62 K in $[\text{Dy}(\text{Cp}^{\text{iPr4Me}})_2]^+$, the result being attributed to the elimination of C-H bending modes that are responsible for mediating spin relaxation.²⁰ Similarly, replacing the tri(*tert*-butyl)cyclopentadienyl ligand with penta(isopropyl)cyclopentadienyl and penta(methyl)cyclopentadienyl ligands results in an increase in the 100-s blocking temperature from 53 K in $[\text{Dy}(\text{Cp}^{\text{tBu}})_2]^+$ to 65 K in $[\text{Dy}(\text{Cp}^{\text{iPr5}})(\text{Cp}^{\text{Me5}})]^+$.^{21,22} However, changes to the steric and electronic environment upon ligand substitution complicate an in depth analysis of this effect. As such, it has

been proposed that isotopic substitution is perhaps the only rigorous way to prove the effect of spin-vibronic coupling; however, this idea has not yet been experimentally realized.⁸

Lunghi, Sessoli, and coworkers derived a spin-vibronic relaxation time given by eqn (1):

$$\tau = \frac{\hbar\omega}{V^2} \exp\left(\frac{\hbar\omega}{2k_B T}\right) \quad (1)$$

where ω is the angular frequency of the vibrational mode coupling to the spin transition, V is the spin-vibronic coupling strength, k_B is the Boltzmann constant, T is the temperature, and \hbar is Planck's constant.^{12,13} It is immediately evident from this equation that increasing the vibrational frequency, ω , should increase the relaxation time, and thus rigid molecular magnets with high vibrational frequencies should be targeted. On the other hand, spin relaxation time can be controlled by spin-vibronic coupling strength, V , which is modulated by structural changes affecting magnetic anisotropy.²³ For an $S = 1/2$ system, magnetic anisotropy arises from the anisotropy of the g factor, which is proportional to ζ/δ , where ζ is the effective spin-orbit coupling constant and δ is the excited state energy separation.²⁴ For $S > 1/2$, magnetic anisotropy arises from zero-field splitting, given by $D \propto \zeta^2/\delta$.²⁵ This implies that V scales with ζ/δ (for an $S = 1/2$ system) or ζ^2/δ (for an $S > 1/2$ system). Thus, it follows from eqn (1) that relaxation time should be proportional to $(\zeta/\delta)^{-2}$ for an $S = 1/2$ system and $(\zeta^2/\delta)^{-2}$ for an $S > 1/2$ system. Therefore, the ability to tune the spin-vibronic relaxation time via the spin-orbit coupling constant would present a valuable new handle for manipulating spin relaxation in paramagnetic molecules.

We previously reported the first paramagnetic zero-valent transition metal isocyanide complex $V(\text{CNXyl})_6$ ($\text{CNXyl} = 2,6\text{-dimethylphenyl isocyanide}$)²⁶ and more recently the synthesis of paramagnetic $\text{Nb}(\text{CNDipp})_6$ and $\text{Ta}(\text{CNDipp})_6$ complexes ($\text{CNDipp} = 2,6\text{-diisopropylphenyl isocyanide}$),^{27,28} the first zero-valent niobium and tantalum isocyanide analogs of the highly unstable molecules $\text{Nb}(\text{CO})_6$ and $\text{Ta}(\text{CO})_6$. These complexes possess low-spin ($S = 1/2$) d^5 electron configurations that provide a platform for studying spin-vibronic relaxation without complications from relaxation through magnetic excited states. Access to an isostructural series of 3d, 4d, and 5d metal ions would further enable an unprecedented study of the impact of varying spin-orbit coupling strength on this relaxation. Herein, we report the synthesis of $V(\text{CNDipp})_6$ and the spectroscopic and magnetic study of the isostructural, isoelectronic triad $M(\text{CNDipp})_6$ ($M = \text{V}$ (**1**), Nb (**2**), Ta (**3**)), and show that all three complexes exhibit slow magnetic relaxation of molecular origin. To the best of our knowledge, this result marks the first observation of slow magnetic relaxation in niobium and tantalum molecular complexes.²⁹ More importantly, our results highlight the influence of spin-orbit coupling interaction on spin-vibronic relaxation, and we find that the spin-vibronic relaxation time is inversely proportional to the square of the magnitude of the spin-orbit coupling.

Results and Discussion

Synthesis and Structural Characterization. The synthesis of $V(\text{CNDipp})_6$ (**1**) was carried out via a similar route to that reported previously for the synthesis of $V(\text{CNXyl})_6$.²⁶ Briefly,

$V(\text{C}_{10}\text{H}_7\text{Me})_2$ ($\text{C}_{10}\text{H}_7\text{Me}^- = 1\text{-methyl-naphthalenide}$) was generated *in situ* from the reaction of $\text{NaC}_{10}\text{H}_7\text{Me}$ and $\text{VCl}_3(\text{THF})_3$ ($\text{THF} = \text{tetrahydrofuran}$), and subsequent reaction with CNDipp in THF afforded **1** as a golden-brown microcrystalline solid. The compounds $\text{Nb}(\text{CNDipp})_6$ (**2**) and $\text{Ta}(\text{CNDipp})_6$ (**3**) were prepared as previously described.^{27,28} Single crystals of compound **1** were grown from a THF solution layered with pentane and stored at -10°C . Single-crystal X-ray diffraction characterization revealed that **1** crystallizes in the space group $R\bar{3}$ (Figure 1) and is isostructural to **2** and **3**, with an asymmetric unit that contains one sixth of the metal atom and one CNDipp ligand. Consequently, all three molecules adopt a perfect trigonal antiprismatic D_{3d} symmetry, as dictated by the crystallographic three-fold rotational axis and inversion center. The compounds can also be viewed as distorted octahedra that are axially compressed along the three-fold axis. The C-M-C angles where the two C atoms are related by a three-fold rotation are $94.67(6)$, $95.46(6)$, and $93.93(5)^\circ$ for **1**, **2**, and **3**, respectively.^{27,28}

For a low-spin, octahedral d^5 complex, the $(t_{2g})^5$ electronic configuration with ${}^2T_{2g}$ electronic state is subject to Jahn-Teller distortion. Compression along the three-fold axis (z axis) causes destabilization of the a_1 orbital, resulting in a $(e^4)(a_1)^1$ electronic configuration and a ${}^2A_{1g}$ electronic ground state. Interestingly, a trigonal distortion of the isolobal $V(\text{CO})_6$ complex to D_{3d} symmetry was computationally predicted and spectroscopically detected at 4 K, but the molecule is highly fluxional at elevated temperature.^{30,31} Given that complexes **1**–**3** all adopt D_{3d} symmetry in the solid state, they are expected to have a larger Jahn-Teller energy stabilization (see below).

Cyclic voltammograms collected for **1**–**3** in 1,2-difluorobenzene revealed reversible, one-electron reduction events at -2.15 , -2.01 , and -2.03 V vs. $[\text{FcCp}_2]^{+/0}$, respectively, corresponding to the generation of stable 18-electron $[M(\text{CNDipp})_6]^-$ species (Figure S5), of which the Ta congener has been previously isolated.²⁸ Cyclic voltammograms collected for **1** and $V(\text{CNXyl})_6$ also feature two oxidation events at more positive potentials, suggesting that stable $V(\text{I})$ and $V(\text{II})$

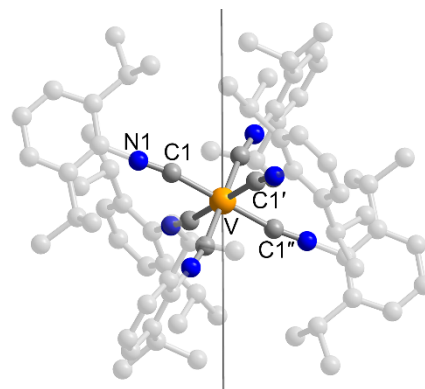


Figure 1. Solid-state structure of $V(\text{CNDipp})_6$ (**1**) determined at 173 K. Orange, blue, and gray spheres represent V, N, and C atoms, respectively. A gray vertical line denotes the crystallographic c axis (-3 axis). The disordered component and H atoms are omitted for clarity. Selected bond distances and angles: V-C1 $2.0138(16)$ Å, $\text{C1-V-C1}'$ $94.67(6)^\circ$, $\text{C1}'\text{-V-C1}''$ $85.33(6)^\circ$, V-C1-N1 $169.0(4)^\circ$, where ' denotes a three-fold rotation and '' denotes an inversion operation, respectively.

species may be accessible (Figure S6). Indeed, $[\text{V}(\text{CNXyl})_6]^-$ and $[\text{V}(\text{CNXyl})_6]^+$ have previously been isolated.²⁶

Electron Paramagnetic Resonance Spectroscopy. EPR spectra collected on microcrystalline powder samples of **1–3** feature axial signals as a result of the Jahn-Teller compression along a trigonal axis (Figure 2). For a low-spin d^5 complex in trigonal symmetry, the g factor can be expressed as:²⁴

$$g_{\perp} = 1 + \frac{1+3\eta/2}{\Lambda} \quad (2)$$

$$g_{\parallel} = -1 + \frac{3(1-\eta/2)}{\Lambda} \quad (3)$$

where $\eta = \zeta/\delta$ is the ratio of spin-orbit coupling constant (ζ) to the trigonal energy splitting of the t_2 orbitals (δ), and $\Lambda = \sqrt{1 - \eta + 9\eta^2/4}$.²⁴ The g_{\perp} values increase from 2.065 to 2.168 to 2.372, while the g_{\parallel} values decrease from 2.002 to 1.966 to 1.642 in going from V to Nb to Ta. The trend in the g_{\perp} and g_{\parallel} values for **1–3** reveals the expected increase in spin-orbit coupling as the atomic number increases from V to Ta. The η ratio deduced from experimental g factors and from eqns (2) and (3) unambiguously shows this increase in spin-orbit coupling (Figure 2 inset and Table 1). We note that deviation of experimental g values from the calculated values may be attributed to covalency due to significant metal–ligand π backbonding (see below).

The EPR spectra of crystalline samples of **1–3** only exhibit broad features with no evidence of hyperfine interactions between the unpaired electron and metal nuclear spins, which may be explained by exchange narrowing.³² Exchange narrowing is further implicated by the observed lineshapes, which appear to be Lorentzian and are not well modeled away from

Table 1 EPR Simulation Parameters for Complexes 1–3 and the Corresponding Spin-Orbit Coupling Constant and Energy Splitting Ratios

	g_{\parallel}	g_{\perp}	$\eta = \zeta/\delta$
V(CNDipp) ₆ (1)	2.002	2.065	0.02
Nb(CNDipp) ₆ (2)	1.966	2.168	0.09
Ta(CNDipp) ₆ (3)	1.642	2.372	0.26

the resonance field by the fitting program, which uses a Pilmrow (Gaussian) lineshape. In contrast, EPR spectra obtained for frozen toluene solutions of **1–3** exhibit the expected splitting due to hyperfine interactions with ⁵¹V ($I = 7/2$), ⁹³Nb ($I = 9/2$), and ¹⁸¹Ta ($I = 7/2$) nuclei, respectively (Figs. S7–S9). However, the simulated g -values for the solution state spectra (Table S5) differ from those in the solid-state, indicating that the complexes adopt different geometries in solution. Consequently, the frozen solution EPR spectra will not be discussed further. Additionally, although the diamagnetic congeners $M'(\text{CNDipp})_6$ ($M' = \text{Cr},^{33} \text{W}^{34}$) of complexes **1** and **3** are known, they crystallize in different space groups and with packing schemes. Thus, dilution via co-crystallization in a diamagnetic matrix would involve a structural change non-native to the pristine solid samples, preventing further EPR experiments. Finally, we note that the analogous V(CNXyl)₆ complex was found to be EPR silent at 293 K in toluene solution due to fast paramagnetic relaxation associated with the low-spin d^5 configuration.²⁶ The EPR spectrum of the complex was re-investigated in this work, and a signal was observed at the much lower temperature of 25 K (Figure S10).

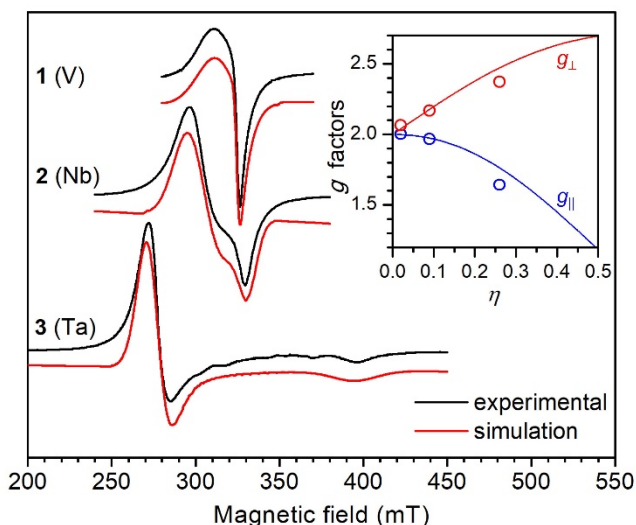


Figure 2. X-band EPR spectra of crystalline samples of **1–3**. Spectra of **1** and **2** were measured at 5 K, and that of **3** at 3 K. Experimental spectra are shown as black lines, and simulation are plotted in red. Inset: Dependence of the g factors on η according to Eqns. (2) and (3) (red and blue lines, respectively). Experimental g values are plotted in open circles.

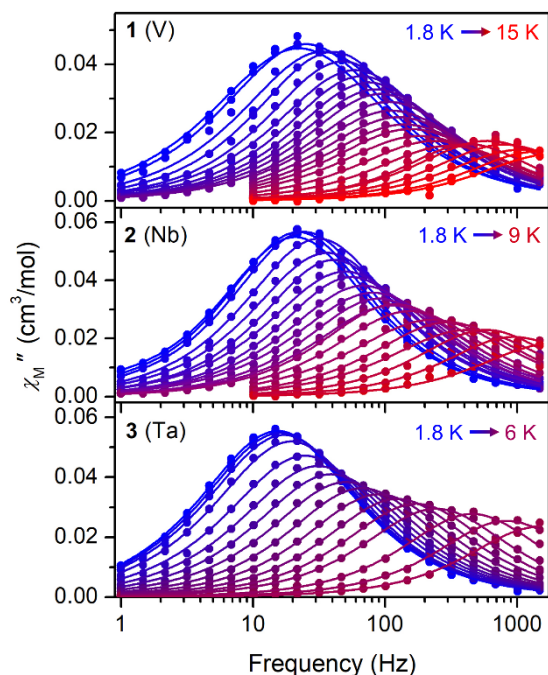


Figure 3. Variable-temperature out-of-phase magnetic susceptibility data for **1** (top) and **2** (center) collected under $H_{dc} = 2500$ Oe, and **3** (bottom) collected under $H_{dc} = 2000$ Oe. Solid lines are fit to the data according to a generalized Debye model.⁴

Magnetic Measurements. Dc magnetic susceptibility data were collected for microcrystalline powder samples of **1** and **2** under an applied field of 1000 Oe. Static magnetic susceptibility data previously reported for **3**²⁸ are also discussed here for comparison. At 2 K, the $\chi_M T$ products of **1**, **2**, and **3** are 0.434, 0.336, and 0.387 $\text{cm}^3\text{K/mol}$, respectively (Figure S11), consistent with an orbital singlet $^2A_{1g}$ ground state of a statically Jahn-Teller distorted octahedral complex ($\chi_M T = 0.375$ $\text{cm}^3\text{K/mol}$). Deviations from the expected value are likely due to the anisotropic g factors of these complexes, magnetic torquing of the samples, and possible small errors associated with measurements of sample mass and corresponding diamagnetic corrections, which will be more significant in low-spin compounds bearing large diamagnetic ligands. For all compounds, $\chi_M T$ increases linearly with temperature (with slight deviation of unknown origin for **2**), which is characteristic of temperature-independent paramagnetism, consistent with the presence of low-lying excited states with large orbital contributions.³⁵ The 2E_g electronic excited states in **1**, **2**, and **3** are calculated to be 1912, 1902, and 1143 cm^{-1} above the ground state, respectively (see below). This low-lying excited state bearing orbital angular momentum mixes significantly with the ground $^2A_{1g}$ state in **1–3**, creating anisotropy in the g factor as observed in the EPR spectra. This result further suggests that slow magnetic relaxation might be observed in these complexes due to anisotropy from excited state orbital degeneracy.³⁶ Indeed, ac magnetic susceptibility data collected for **1–3** under optimal dc fields of 2000 or 2500 Oe feature temperature-dependent signals in the out-of-phase susceptibility (χ_M''), confirming slow magnetic relaxation of molecular origin via spin-phonon processes (Figure 3).

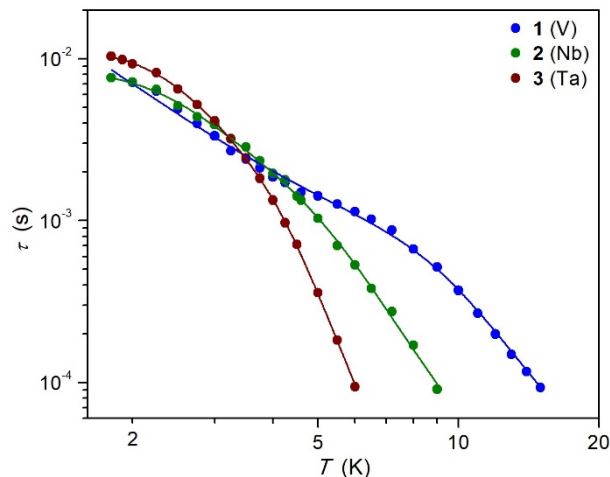


Figure 4. Plots of the relaxation time, τ (log scale) versus temperature (log scale) for **1** (blue) and **2** (green), measured under $H_{dc} = 2500$ Oe, and **3** (dark red) under $H_{dc} = 2000$ Oe. Solid lines are fits to the data.

Relaxation times, τ , were extracted from fits to the ac susceptibility data using a generalized Debye model.⁴ A plot of τ vs T for **1–3** is shown in Figure 4. At low temperatures, the temperature dependence of τ is indicative of spin-spin relaxation, as commonly observed in other $S = 1/2$ compounds.^{37,38} However, relaxation times for **1–3** begin to deviate above 5 K, where spin-phonon relaxation starts to dominate as phonons with energy sufficient to initiate the activated relaxation pathway become thermally available. Two key observations can be made regarding the relaxation behavior at these temperatures. First, compound **1** exhibits the slowest relaxation for a given temperature, followed by **2** and then **3**. For example, at 6 K, $\tau = 1.14$, 0.53, and 0.11 ms for **1–3**, representing an order of magnitude increase in the relaxation time simply by changing the identity of the metal center. Second, the slope of τ versus T increases from **1** to **3**, and thus relaxation becomes more rapid with increasing temperature upon progressing from V to Ta. The temperature dependence of τ correlates with the spin-vibronic coupling strength,²³ and thus spin-vibronic coupling for these compounds follows the trend Ta > Nb > V. This observation coincides with the trend in the g values across the series of compounds, indicating that, in the temperature regime at which spin-vibronic relaxation is dominant, the relaxation time for this system scales with the spin-orbit coupling interaction. Fitting of relaxation times to Eq. (1) was attempted to extract quantitative information about the spin-vibronic coupling strength, V (see Supporting Information), as well as phonon frequencies. The results are listed in Tables 3 and S10. We however note the large uncertainties associated with the fit (Table S9), precluding definitive quantitative analysis.

Electronic Structure Computation. Density functional theory calculations were performed on **1**, **2**, and **3** to investigate the electronic structure of the complexes. Geometry optimization was initially performed due to disorder in the crystal structures. Single point calculations on the optimized geometries give Löwdin spin populations on the metal centers of 0.834, 0.658, and 0.512 for **1**, **2**, and **3**, respectively, indicating an increase in spin delocalization upon going to heavier metals. Singly-occupied molecular orbital plots depict the distri-

Table 2 Energies of Non-Relativistic and Relativistic (Spin-Orbit Coupled) States (cm^{-1}) of $\text{M}(\text{CNPh})_6$ from CASSCF Calculations, and Computed and Experimental g -Factors for the Γ_{4g} Ground State Kramers Doublet

	V(CNPh) ₆	Nb(CNPh) ₆	Ta(CNPh) ₆
² A _{1g}	0	0	0
² E _g	1912	1902	1143
Γ_{4g}	0	0	0
Γ_{5g}	1874	1826	1380
Γ_{6g}	1957	2022	1804
ζ_{eff}	81 (114) ^a	187 (375) ^a	378 (1538) ^a
g_{\parallel}	1.996 (2.002) ^b	1.958 (1.966) ^b	0.815 (1.642) ^b
g_{\perp}	2.086 (2.065) ^b	2.213 (2.168) ^b	2.564 (2.372) ^b

Symmetry notation pertain to the trigonal D_{3d} (²A_{1g} and ²E_g spin-free non-relativistic states) and the D_{3d}^* double group (Γ_{4g} , Γ_{5g} , and Γ_{6g} spin-orbit coupled states). ^aFree atom values computed from CASSCF calculations. ^bValues obtained from simulating EPR spectra.

bution of the single spin over the metal atom and the isocyanide ligands (Figure S24, top), supporting the π backbonding ability of the isocyanide ligands to stabilize low valent metal complexes. Attempts to compute a spin configuration in which the transition metal is oxidized while the ligands are reduced failed. Therefore, it follows that CNDipp behaves as a redox innocent ligand, rendering an oxidation state of zero for V, Nb, and Ta.

Subsequently, the sublevels of the ²T_{2g} ground state were computed using the complete active space self-consistent field modulated by second-order N -electron valence perturbation theory (CASSCF/NEVPT2), as performed on the truncated model complexes $\text{M}(\text{CNPh})_6$ ($\text{M} = \text{V}, \text{Nb}, \text{Ta}$; CNPh = phenyl isocyanide). Convergence of CASSCF was achieved using the CAS(5,12) active space. Figure S25 depicts the molecular orbital plots of the magnetic orbital and its antibonding congener for Ta(CNPh)₆. The single spin resides on a $5d_{z^2}$ orbital engaged in Ta–C π backbonding. The Ta center is in a formally zero oxidation state with the single unpaired electron shared almost equally between the Ta $5d_{z^2}$ orbital and the π^* orbitals of CNPh ligands. Using this extended charge transfer model, the energies of the three sublevels of the octahedral ²T_{2g} ground state were successfully computed, of which its degeneracy is broken by the D_{3d} symmetry of the complex. A non-relativistic calculation was followed by accounting for spin-orbit coupling using quasi-degenerate perturbation theory (QDPT) to afford expectation values for the Zeeman operator and anisotropic g factors (Table 2). In D_{3d} symmetry, the ²A_{1g} ground state is separated from the ²E_g excited state by an energy gap of 1912 (V), 1902 (Nb) and 1143 cm^{-1} (Ta) according to the results of the CASSCF calculation. Accounting for dynamic correlation using NEVPT2 does not appreciably affect these energies. Effective spin-orbit coupling parameters extracted from the relativistic calculation are 81 (V), 187 (Nb), and 378 cm^{-1} (Ta), revealing significant reductions of 29%, 50%, and 75%, respectively, relative to the free ion values. This reflects the increasing metal–ligand covalency in the se-

ries. The calculated g factors reproduced reasonably well the experimental value (Table 2). Deviations between computed and experimental data increase from V to Ta, as expected since dynamical correlation for heavier elements becomes increasingly more important. Our methods, being based on post-Hartree-Fock calculations, underestimate dynamical correlations for heavier metals.

Jahn-Teller Distortion and Spin-Phonon Coupling. Octahedral complexes with ²T_{2g} ground states are geometrically unstable with respect to nuclear displacements along the ϵ_g stretching and τ_{2g} bending modes. Previous work on hexacyano complexes of first-row transition metals showed that τ_{2g} distortion is energetically favored.³⁹ Coupling of the τ_{2g} mode with the ²T_{2g} ground state leads to trigonal D_{3d} geometries with four trigonal axes perpendicular to each trigonal face of the octahedron (Figure S26). Depending on the donor properties of the ligand, trigonal elongation (for π donor ligands) or trigonal compression (for π acceptor ligands) are possible. In agreement with the π backbonding character of the CNDipp ligands, trigonally compressed geometries are observed in all complexes **1–3**. Using the distortion obtained from DFT-optimized geometry and the CASSCF-computed ²A_{1g} and ²E_g energies, we extract the linear Jahn-Teller coupling constant (V) of 4395, 3474, and 2920 $\text{cm}^{-1}/\text{\AA}$ for V(CNPh)₆, Nb(CNPh)₆, and Ta(CNPh)₆, respectively (see Supporting Information for more details). The decrease of linear vibronic coupling constants reflects a weakening of vibronic coupling, opposing the increase in effective spin-orbit coupling constants. Finally, the Jahn-Teller stabilization energy (E_{JT}) can be computed from the energy difference of the octahedral and trigonally distorted geometries, to be 537, 732, and 381 cm^{-1} for V(CNPh)₆, Nb(CNPh)₆, and Ta(CNPh)₆, respectively. The ratios $E_{JT}/\zeta_{\text{eff}}$ of 7.9, 3.9, and 1.0 were obtained for V, Nb, and Ta, respectively. We note these ratios are larger for V(CNPh)₆ and Nb(CNPh)₆ than for their carbonyl congeners (~ 3.77 – 3.98 for V(CO)₆ and ~ 2.80 – 2.90 for Nb(CO)₆; the value for Ta(CO)₆ has not been reported).³¹ When $E_{JT}/\zeta > 0.75$, that is, when the Jahn-Teller stabilization energy is comparable with or exceeds the spin-orbit coupling, a structural distortion is predicted to give rise to a D_{3d} (or D_{4h}) geometry as the ground state.^{31,40} This relationship holds true for V(CNPh)₆, Nb(CNPh)₆, and Ta(CNPh)₆, rationalizing the observed trigonal distortion in the solid-state structures of **1–3**. We note that the elusive Ta(CO)₆ complex is predicted to resist Jahn-Teller distortion due to a small, estimated E_{JT}/ζ value of ~ 0.25 ,³¹ in contrast to what is seen here for Ta(CNDipp)₆.

Using the force constants from Jahn-Teller analysis, we compute the frequency of the τ_{2g} normal mode to be 70, 52, and 57 cm^{-1} for V(CNPh)₆, Nb(CNPh)₆, and Ta(CNPh)₆, respectively. These values agree intriguingly well with the values extracted from fitting magnetic relaxation time $\tilde{\nu}_1 = 89, 59, 66 \text{ cm}^{-1}$ for **1–3**, respectively (Table 3).

To calculate spin-phonon coupling parameters, first principles spin-phonon calculations were performed on the free molecules without taking into account solid-state effects, such as phonon dispersion and the multitude of molecular and lattice modes which can also contribute to the relaxation mechanism. The single effective mode approach⁴⁰ was used, wherein molecular and lattice vibrations are projected onto a single mode,

Table 3 Spin-Phonon Coupling Parameters and Magnetic Relaxation Times Computed on Model Complexes M(CNPh)₆ and Experimentally Determined by Fitting AC Susceptibility Data of M(CNDipp)₆

	V(CNPh) ₆	Nb(CNPh) ₆	Ta(CNPh) ₆
$(\partial g_{\perp} / \partial Q)_{\perp}$	0.0129	0.0218	0.0557
V_{calc} (cm ⁻¹)	1.8×10^{-3}	2.9×10^{-3}	6.05×10^{-3}
$\tilde{\nu}_{\text{calc}}$ (cm ⁻¹)	70	52	57
τ_{calc} (ms) at 6 K	36.1	3.1	1.1
	V(CNDipp) ₆	Nb(CNDipp) ₆	Ta(CNDipp) ₆
V_1 (cm ⁻¹)	$1.7(3) \times 10^{-2}$	$1.7(3) \times 10^{-2}$	$9(1) \times 10^{-2}$
$\tilde{\nu}_1$ (cm ⁻¹)	89(6)	59(4)	66(2)
τ (ms) at 6 K	1.14	0.53	0.11

which in this case is taken to be the Jahn-Teller active vibration, Q , (Figure S27). It is this vibration that undergoes a softening, affecting the coupling of the spin with its surrounding CNPh ligands. Assuming that magnetic relaxation is mostly affected by spin flipping via the transverse magnetic field, the first derivatives of g_{\perp} with respect to normal mode Q , for the three model complexes were numerically computed (Table 3). Spin-phonon coupling parameters V were calculated using $B = 2500$ Oe (for V and Nb) or 2000 Oe (for Ta) according to Eqn. 4 (see Supporting Information for a derivation):

$$V = \mu_B \left(\frac{\partial g_{\perp}}{\partial Q_{\tau}} \right)_0 B \quad (4)$$

Table 3 lists the calculated and experimental spin-phonon coupling constants and relaxation times at 6 K. Despite using truncated model complexes, the agreement between computed and experimental parameters is impressive, providing evidence for the importance of spin-orbit coupling in modulating spin-vibronic relaxation. Figure 5 illustrates the linear empirical relationship between the calculated spin-phonon coupling constant, V_{calc} , and the effective spin-orbit coupling constant. More intriguing are the linear relationship between V_{calc} and η and the linear relationship of relaxation rate with both ζ_{eff}^2 and η^2 , which corroborates the theoretical model from the *ab initio* study (see eqn (1) and discussion above).^{12,13} Finally, we note that spin-orbit coupling is not the only factor affecting the magnetic relaxation, but Jahn-Teller coupling which decrease from V and Nb toward the Ta complex partially opposes the spin-orbit coupling effect. Metal–ligand covalency which increases toward Ta may also contribute to the increase in relaxation rate in these complexes.

Conclusions

The foregoing spectroscopic and magnetic data for the isoelectronic, isostructural series M(CNDipp)₆ (M = V (1), Nb (2), Ta (3)) coupled with first principle spin-phonon computations provide clear evidence that spin-vibronic coupling scales with the magnitude of the spin-orbit coupling interaction, and corroborate the proposal that relaxation time in $S = 1/2$ molecules can be prolonged by using lighter elements.¹³ This finding has direct relevance for the development of long-lived spin-based qubits. Meanwhile, efforts to maximize magnetic anisotropy in single-molecule magnets through spin-orbit coupling interaction must be weighed against the increasingly dominant spin-vibronic coupling, which can favor rapid relaxation. Accordingly, mitigation of spin-vibronic relaxation in heavy transition metal-based, and even actinide-based, single-molecule magnets must be taken into consideration.

ASSOCIATED CONTENT

The Supporting Information is available free of charge at <http://pubs.acs.org>.

Experimental details and materials characterization, crystallographic information, electrochemical data, additional spectroscopic and magnetic data, computational details.

AUTHOR INFORMATION

Corresponding Author

Frank Neese – Max-Planck Institut für Kohlenforschung, Kaiser-Wilhelm-Platz 1, D-45470 Mülheim an der Ruhr, Germany

Email: neese@kofo.mpg.de

Jeffrey R. Long – Department of Chemistry and Department of Chemical and Biomolecular Engineering, University of California, Berkeley, Berkeley, California 94720, United States; Materials Sciences Division, Lawrence Berkeley National Laboratory, Berkeley, California 94720, United States

Email: jrlong@berkeley.edu

Authors

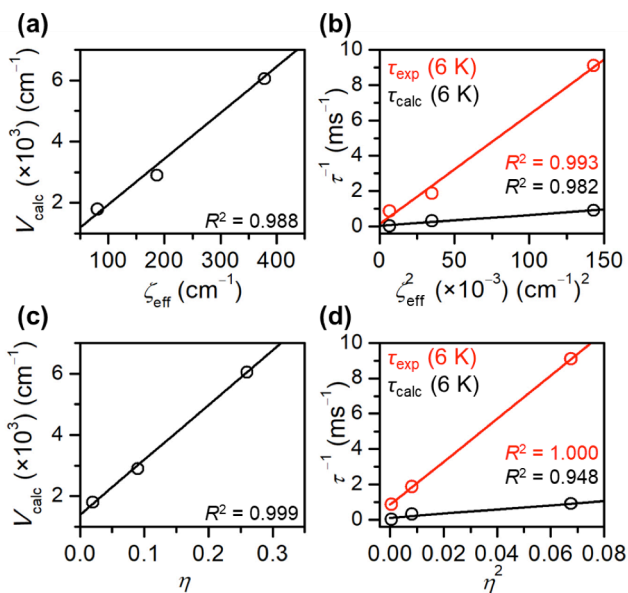


Figure 5. (a) Plot of calculated V vs calculated ζ_{eff} . (open circles) with a linear fit (solid line). (b) Plot of experimental (red circles) and calculated (black circles) relaxation rate τ^{-1} at 6 K vs ζ_{eff}^2 of M(CNDipp)₆ and M(CNPh)₆ (M = V, Nb, Ta), respectively. Solid lines are linear fit. (c) Plot of calculated V vs experimental $\eta = \zeta/\delta$ extracted from EPR data. (d) Plot of experimental and calculated τ^{-1} vs η^2 . Experimental V_1 are not plotted due to large uncertainties associated with the data analysis.

Khetpakorn Chakarawet – Department of Chemistry, University of California, Berkeley, Berkeley, California 94720, United States

Mihail Atanasov – Max-Planck Institut für Kohlenforschung, Kaiser-Wilhelm-Platz 1, D-45470 Mülheim an der Ruhr, Germany; Institute of General and Inorganic Chemistry, Bulgarian Academy of Science, Akad. G. Bontchev Street, Bl.11, 1113 Sofia, Bulgaria

John E. Ellis – Department of Chemistry, University of Minnesota, Minneapolis, Minnesota 55455, United States

Wayne W. Lukens Jr. – Chemical Sciences Division, Lawrence Berkeley National Laboratory, Berkeley, California 94720, United States

Victor G. Young Jr. – Department of Chemistry, University of Minnesota, Minneapolis, Minnesota 55455, United States

Ruchira Chatterjee – Molecular Biophysics and Integrated Bioimaging Division, Lawrence Berkeley National Laboratory, Berkeley, California 94720, United States

Author Contributions

The manuscript was written through contributions of all authors. All authors have given approval to the final version of the manuscript.

ACKNOWLEDGMENT

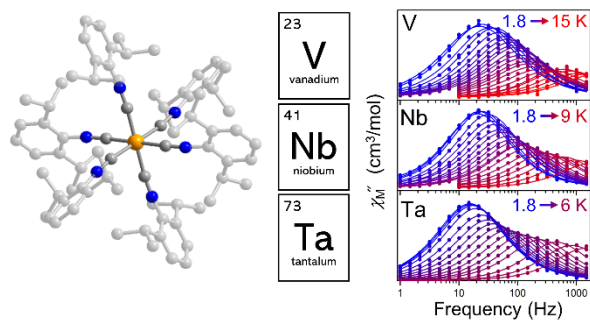
This research was funded by NSF Grants CHE-1800252 and CHE-2102603. J.E.E. thanks Research Gift Support, administered by the University of Minnesota Foundation. EPR spectroscopy and analysis (W.W.L. and R.C.) were supported by U.S. Department of Energy, Basic Energy Sciences, Chemical Sciences, Biosciences, and Geosciences Division and were performed at Lawrence Berkeley National Laboratory under Contract No. DE-AC02-05CH11231. V.G.Y. Jr. thanks the National Science Foundation for a Major Research Instrumentation award (CHE-1229400) in the acquisition of the crystal diffractometer employed in the X-ray diffraction study. We further thank the government of Thailand for support of K.C. through the Development and Promotion of Science and Technology (DPST) scholarship and Dr. Katie R. Meihaus for editorial assistance.

REFERENCES

- (1) McMahon, K. L.; Cowin, G.; Galloway, G. Magnetic Resonance Imaging: The Underlying Principles. *J. Orthop. Sport. Phys. Ther.* **2011**, *41*, 806–819.
- (2) Layfield, R. A. Organometallic Single-Molecule Magnets. *Organometallics* **2014**, *33*, 1084–1099.
- (3) Ariciu, A.-M.; Woen, D. H.; Huh, D. N.; Nodaraki, L. E.; Kostopoulos, A. K.; Goodwin, C. A. P.; Chilton, N. F.; McInnes, E. J. L.; Winpenny, R. E. P.; Evans, W. J.; et al. Engineering Electronic Structure to Prolong Relaxation Times in Molecular Qubits by Minimising Orbital Angular Momentum. *Nat. Commun.* **2019**, *10*, 3330.
- (4) Gatteschi, D.; Sessoli, R.; Villain, J. *Molecular Nanomagnets*; Oxford Univ. Press, 2006.
- (5) Rinehart, J.; Long, J. Exploiting Single-Ion Anisotropy in the Design of f-Element Single-Molecule Magnets. *Chem. Sci.* **2011**, *2*, 2078.
- (6) Sessoli, R.; Gatteschi, D.; Caneschi, A.; Novak, M. A. Magnetic Bistability in a Metal-Ion Cluster. *Nature* **1993**, *365*, 141–143.
- (7) Aravena, D.; Ruiz, E. Spin Dynamics in Single-Molecule Magnets and Molecular Qubits. *Dalton Trans.* **2020**, *49*, 9916–9928.
- (8) Escalera-Moreno, L.; Baldoví, J. J.; Gaita-Ariño, A.; Coronado, E. Spin States, Vibrations and Spin Relaxation in Molecular Nanomagnets and Spin Qubits: A Critical Perspective. *Chem. Sci.* **2018**, *9*, 3265–3275.
- (9) Gatteschi, D.; Sessoli, R. Quantum Tunneling of Magnetization and Related Phenomena in Molecular Materials. *Angew. Chem. Int. Ed.* **2003**, *42*, 268–297.
- (10) Harman, W. H.; Harris, T. D.; Freedman, D. E.; Fong, H.; Chang, A.; Rinehart, J. D.; Ozarowski, A.; Sougrati, M. T.; Grandjean, F.; Long, G. J.; et al. Slow Magnetic Relaxation in a Family of Trigonal Pyramidal Iron(II) Pyrrolide Complexes. *J. Am. Chem. Soc.* **2010**, *132*, 18115–18126.
- (11) Meihaus, K. R.; Long, J. R. Magnetic Blocking at 10 K and a Dipolar-Mediated Avalanche in Salts of the Bis(η^8 -Cyclooctatetraenide) Complex $[\text{Er}(\text{COT})_2]^-$. *J. Am. Chem. Soc.* **2013**, *135*, 17952–17957.
- (12) Lunghi, A.; Totti, F.; Sessoli, R.; Sanvito, S. The Role of Anharmonic Phonons in Under-Barrier Spin Relaxation of Single Molecule Magnets. *Nat. Commun.* **2017**, *8*, 14620.
- (13) Lunghi, A.; Totti, F.; Sanvito, S.; Sessoli, R. Intra-Molecular Origin of the Spin-Phonon Coupling in Slow-Relaxing Molecular Magnets. *Chem. Sci.* **2017**, *8*, 6051–6059.
- (14) Atanasov, M.; Zadrozny, J. M.; Long, J. R.; Neese, F. A Theoretical Analysis of Chemical Bonding, Vibronic Coupling, and Magnetic Anisotropy in Linear Iron(II) Complexes with Single-Molecule Magnet Behavior. *Chem. Sci.* **2013**, *4*, 139–156.
- (15) Moseley, D. H.; Stavretis, S. E.; Thirunavukkuarasu, K.; Ozerov, M.; Cheng, Y.; Daemen, L. L.; Ludwig, J.; Lu, Z.; Smirnov, D.; Brown, C. M.; Pandey, A.; Ramirez-Cuesta, A. J.; Lamb, A. C.; Atanasov, M.; Bill, E.; Neese, F.; Xue, Z.-L. Spin-Phonon Couplings in Transition Metal Complexes with Slow Magnetic Relaxation. *Nat. Commun.* **2018**, *9*, 1–11.
- (16) Yu, K.-X.; Kragoskow, J. G. C.; Ding, Y.-S.; Zhai, Y.-Q.; Reta, D.; Chilton, N. F.; Zheng, Y.-Z. Enhancing Magnetic Hysteresis in Single-Molecule Magnets by Ligand Functionalization. *Chem* **2020**, *6*, 1777–1793.
- (17) Bone, A. N.; Widener, C. N.; Moseley, D. H.; Liu, Z.; Lu, Z.; Cheng, Y.; Daemen, L. L.; Ozerov, M.; Telsler, J.; Thirunavukkuarasu, K.; Smirnov, D.; Greer, S. M.; Hill, S.; Krzystek, J.; Holldack, K.; Aliabadi, A.; Schnegg, A.; Dunbar, K. R.; Xue, Z. Applying Unconventional Spectroscopies to the Single - Molecule Magnets, $\text{Co}(\text{PPh}_3)_2 \text{X}_2$ ($\text{X}=\text{Cl}, \text{Br}, \text{I}$): Unveiling Magnetic Transitions and Spin - Phonon Coupling. *Chem. – A Eur. J.* **2021**, *27* (43), 11110–11125.
- (18) Lunghi, A.; Sanvito, S. Multiple Spin-Phonon Relaxation Pathways in a Kramer Single-Ion Magnet. *J. Chem. Phys.* **2020**, *153*, 174113.
- (19) Briganti, M.; Santanni, F.; Tesi, L.; Totti, F.; Sessoli, R.; Lunghi, A. A Complete Ab Initio View of Orbach and Raman Spin-Lattice Relaxation in a Dysprosium Coordination Compound. *J. Am. Chem. Soc.* **2021**, *143*, 13633–13645.
- (20) McClain, R. K.; Gould, C. A.; Chakarawet, K.; Teat, S. J.; Groshens, T. J.; Long, J. R.; Harvey, B. G. High-Temperature Magnetic Blocking and Magneto-Structural Correlations in a Series of Dysprosium(III) Metallocene Single-Molecule Magnets. *Chem. Sci.* **2018**, *9*, 8492–8503.
- (21) Goodwin, C. A. P.; Ortu, F.; Reta, D.; Chilton, N. F.; Mills, D. P. Molecular Magnetic Hysteresis at 60 Kelvin in Dysprosocenium. *Nature* **2017**, *548*, 439–442.
- (22) Guo, F.-S.; Day, B. M.; Chen, Y.-C.; Tong, M.-L.; Mansikkamäki, A.; Layfield, R. A. Magnetic Hysteresis up to 80 Kelvin in a Dysprosium Metallocene Single-Molecule Magnet. *Science* **2018**, *362*, 1400–1403.
- (23) Albino, A.; Benci, S.; Tesi, L.; Atzori, M.; Torre, R.; Sanvito, S.; Sessoli, R.; Lunghi, A. First-Principles Investigation of Spin-Phonon Coupling in Vanadium-Based Molecular Spin Quantum Bits. *Inorg. Chem.* **2019**, *58*, 10260–10268.
- (24) Rieger, P. H. Electron Paramagnetic Resonance Studies of Low-Spin d^5 Transition Metal Complexes. *Coord. Chem. Rev.* **1994**, *135/136*, 203–286.

- (25) Higdon, N. J.; Barth, A. T.; Kozłowski, P. T.; Hadt, R. G. Spin-Phonon Coupling and Dynamic Zero-Field Splitting Contributions to Spin Conversion Processes in Iron(II) Complexes. *J. Chem. Phys.* **2020**, *152*, 204306.
- (26) Barybin, M. V.; Young, V. G.; Ellis, J. E. First Paramagnetic Zerovalent Transition Metal Isocyanides. Syntheses, Structural Characterizations, and Magnetic Properties of Novel Low-Valent Isocyanide Complexes of Vanadium. *J. Am. Chem. Soc.* **2000**, *122*, 4678–4691.
- (27) Kucera, B. E.; Roberts, C. J.; Young, V. G.; Brennessel, W. W.; Ellis, J. E. Niobium Isocyanide Complexes, Nb(CNAr)₆, with Ar = 2,6-Dimethylphenyl (Xyl), a Diamagnetic Dimer Containing Four Reductively Coupled Isocyanides, and Ar = 2,6-Diisopropylphenyl (Dipp), a Paramagnetic Monomer Analogous to the Highly Unstable Hexacarbonyl. *Acta Crystallogr. Sect. C Struct. Chem.* **2019**, *75*, 1259–1265.
- (28) Chakarawet, K.; Davis-Gilbert, Z. W.; Harstad, S. R.; Young, V. G.; Long, J. R.; Ellis, J. E. Ta(CNDipp)₆: An Isocyanide Analogue of Hexacarbonyltantalum(0). *Angew. Chem., Int. Ed.* **2017**, *56*, 10577–10581.
- (29) Wang, X. Y.; Avendaño, C.; Dunbar, K. R. Molecular Magnetic Materials Based on 4d and 5d Transition Metals. *Chem. Soc. Rev.* **2011**, *40*, 3213–3238.
- (30) Parrish, S. H.; Weltner, W. Vanadium and Niobium Hexadinitrogen and Hexacarbonyl Complexes: Electron-Spin-Resonance Spectra at 4 K. *J. Phys. Chem. A* **1999**, *103*, 1025–1028.
- (31) Bernhardt, E.; Willner, H.; Kornath, A.; Breidung, J.; Bühl, M.; Jonas, V.; Thiel, W. *D_{3d}* Ground-State Structure of V(CO)₆: A Combined Matrix Isolation and Ab Initio Study of the Jahn–Teller Effect. *J. Phys. Chem. A* **2003**, *107*, 859–868.
- (32) Abragam, A.; Bleaney, B. *Electron Paramagnetic Resonance of Transition Ions*; Clarendon press, Oxford, 1970.
- (33) Anderson, K. A.; Scott, B.; Wherland, S.; Willett, R. D. Structure of Hexakis(2,6-Diisopropylphenyl Isocyanide)Chromium(0). *Acta Crystallogr. C Cryst.* **1991**, *47*, 2337–2339.
- (34) Sattler, W.; Ener, M. E.; Blakemore, J. D.; Rachford, A. A.; Labeaume, P. J.; Thackeray, J. W.; Cameron, J. F.; Winkler, J. R.; Gray, H. B. Generation of Powerful Tungsten Reductants by Visible Light Excitation. *J. Am. Chem. Soc.* **2013**, *135*, 10614–10617.
- (35) Kahn, O. *Molecular Magnetism*; VCH, 1993.
- (36) Boča, R.; Rajnák, C.; Titiš, J.; Valigura, D. Field Supported Slow Magnetic Relaxation in a Mononuclear Cu(II) Complex. *Inorg. Chem.* **2017**, *56*, 1478–1482.
- (37) Atzori, M.; Tesi, L.; Morra, E.; Chiesa, M.; Sorace, L.; Sessoli, R. Room-Temperature Quantum Coherence and Rabi Oscillations in Vanadyl Phthalocyanine: Toward Multifunctional Molecular Spin Qubits. *J. Am. Chem. Soc.* **2016**, *138*, 2154–2157.
- (38) Atzori, M.; Tesi, L.; Benci, S.; Lunghi, A.; Righini, R.; Taschin, A.; Torre, R.; Sorace, L.; Sessoli, R. Spin Dynamics and Low Energy Vibrations: Insights from Vanadyl-Based Potential Molecular Qubits. *J. Am. Chem. Soc.* **2017**, *139*, 4338–4341.
- (39) Atanasov, M.; Comba, P.; Daul, C. A.; Hauser, A. DFT-Based Studies on the Jahn–Teller Effect in 3d Hexacyanometalates with Orbitally Degenerate Ground States. *J. Phys. Chem. A* **2007**, *111*, 9145–9163.
- (40) Bersuker, I. B.; Blake, A. B. The Jahn–Teller Effect and Vibronic Interactions in Modern Chemistry. *Anal. Chim. Acta* **1987**, *201*, 371

Table of Contents



Zero-valent low-spin group 5 metal triad exhibit slow magnetic relaxation. Spin-orbit coupling plays an important role in facilitating relaxation via spin-vibronic coupling.